JEE Journal of Ecological Engineering

Journal of Ecological Engineering 2024, 25(2), 321–332
https://doi.org/10.12911/22998993/176571
ISSN 2299–8993, License CC-BY 4.0

Received: 2023.11.21
Accepted: 2023.12.20
Published: 2024.01.01

Biosorption of Hexavalent Chromium onto *Ziziphus lotus* Fruits Powder: Kinetics, Equilibrium, and Thermodynamics

Nosair El Yakoubi[1*], Zineb Nejjar El Ansari[1], Mounia Ennami[2], Mohammed L'bachir El Kbiach[1], Loubna Bounab[3], Brahim El Bouzdoudi[1]

[1] Plant Biotechnology Team, Faculty of Sciences, Abdelmalek Essaadi University, Tetouan, Morocco

[2] Agronomic and Veterinary Institute Hassan II, Production, Protection and Plant Biotechnology Department, Rabat, Morocco

[3] Advanced Materials, Structures and Civil Engineering Team, ENSA Tetouan, Abdelmalek Essaadi University, Tetouan, Morocco

* Corresponding author's e-mail: Nosairelyakoubi@gmail.com

ABSTRACT

Ziziphus lotus has been the subject of several researchs because of its nutritional benefits and ecological attributes. The removal of hexavalent chromium Cr(VI) from a solution using powdered *Zizphus lotus* fruits, for its qualities of being inexpensive as well as environmentally friendly, was investigated. The results obtained showed that at pH = 2, at 30°C, after 600 min of adsorbent/adsorbate contact, with 100 mg/L as initial concentration of Cr(VI) and a biosorbent dosage of 5 g/L, the biosorption of Cr(VI) on *Zizphus lotus* fruit powder (ZLFP) is at its maximum rate. The sorption process was exothermic ($\Delta H° = –6.69$ kJ/mol), and was characterized by a positive entropy values ($\Delta S° = 46.76$ J/K mol) suggesting a high affinity of the ZLFP for Cr(VI). Given that the Gibbs free energy ($\Delta G°$) is negative and decreases as temperatures increase from 293 to 323 K, the process of biosorption is both feasible and spontaneous. The Temkin model and the Langmuir model both generated excellent fits to the equilibrium data. The maximum monolayer biosorption capacity was 36.11 mg/g. The pseudo second order model was used to fit the kinetic data relating to the adsorption of Cr(VI) on the ZLFP. The FTIR spectral analysis allowed the characterization of the biochemical groups mainly involved in the sorption of Cr(VI) ions on the ZLFP, and which are: N–C, H-O, O–C, H-C, and O=C. The capacity of *Ziziphus lotus* fruit as an inexpensive, effective, and ecofriendly biosorbent is confirmed through this study.

Keywords: hexavalent chromium, wastewater treatment, *Ziziphus lotus*, kinetic models.

INTRODUCTION

The emergence of life on earth was found to be closely related to the water molecule (White et al. 2020). Human beings owe their survival largely to water (Rosinger and Brewis, 2020). The last century has seen a strong demand for water following the great industrial revolution, often using water, and following the demographic explosion in several corners of the world (Saatsaz, 2020). Thus, domestic activities and industrial activities have largely contributed to water pollution and consequently to the scarcity of drinking water sources available for human consumption (Abdul Maulud et al. 2021). Polluted water effluents contain many types of organic and inorganic chemical contaminants (Elgarahy et al. 2021). Heavy metals form a range of pollutants that have been able to sneak into several natural media such as soils, surface waters, aquifers and many others (Sadeghi et al. 2022). Chromium (Cr) is a metallic element found in the earth's crust in the form of a deposit called Chromite (Coetzee et al. 2020). Depending on their level of oxidation, several forms of chromium can be distinguished, including hexavalent chromium designated by Cr(VI) resulting from the oxidation of trivalent chromium designated by Cr(III). In fact, Cr(VI) is characterized by its high

mobility, reactivity, and ability to cross biological membranes (Mushtaq et al. 2022). Numerous studies have documented the risks associated with Cr(VI) toxicity, including: dysfunction of photosynthesis and growth in plants, mutations, and disturbances of biological functions in humans (Mishra et al. 2019). Depending on the pH of the environment, we can distinguish many molecular species of Cr(VI) in solution (Vu et al. 2019), which are in equilibrium with each other, and which emanate from several anthropogenic activities, such as tanning, metallurgy and electroplating (Ayele and Godeto, 2021).

The direct discharge of polluted effluents is a serious danger threatening environmental health (Tariq et al. 2020). Aquatic environments represent one of the spots where these metallic discharges are discharged, and a wide range of which is bioavailable for the biocenosis and mainly the bioaccumulating organisms (Butnariu, 2022). Thus, the content of toxic metallic elements increases from one link to another along the trophic chains according to a process of biomagnification to reach a threshold that threaten human health (Murtaza et al. 2022).

The scarcity of drinking water, as well as the awareness of the importance of ecosystem health, has stimulated reflections aimed at treating wastewater for its subsequent use for the various sectors requiring water. Thus, several wastewater treatment technologies have been developed and then applied such as: chemical precipitation (Zhang and Duan, 2020), reverse osmosis (Arola et al. 2019), adsorption (Chai et al. 2021), membrane filtration (Hube et al. 2020), and coagulation-flocculation (Jorge et al. 2022). Despite the fact that a number of procedures have undergone testing to determine whether they can remove metallic elements from a metal solution that has been contaminated, adsorption has shown great promise in providing a less expensive, clean and efficient means for metal sequestration (Rashid et al. 2021). The adsorption process is closely linked to the topological and electrical properties of the adsorbent, which is capable of trapping adjacent ionic species by its electrically charged surface patterns distributed over a large surface (Liu et al. 2019). Several studies have focused on exploring the adsorbent properties of biomass, particularly plant biomass, and several types of waste, part of the quest for low-cost and environmentally friendly substances (Boloy et al. 2021). The literature provides a series of biosorbents that have been tested for their biosorption capacity such as: orange peels (Parashar and Gandhimathi, 2022), banana peel (Akpomie and Conradie 2020), brown algae (Jayakumar et al. 2022), bacteria and fungi (Oyewole et al. 2019), etc. By containing a diversity of biochemical molecules such as lignin, polyphenols, polysaccharides, biosorbents of vegetable nature, expose a multitude of chemical functions such as amine groups, phosphate groups, acid groups, sulphonate groups, and hydroxyl groups, capable, thanks to their electrical properties, of carrying out electrostatic interactions with other electrically charged species such as metal ions (Elahi et al. 2020).

The north of Morocco has a great floristic diversity. Thus, shrubs of the Ziziphus lotus species are widely distributed there (El Maaiden et al. 2019). The reproductive phase of this species is characterized by the appearance of a drupe fruit, brown when ripe, within a shrub with multitudes of densely foliated branches. The fruits, locally known as 'Nbeg', are edible either directly or after traditional processing into a flour known as Zemmita (Abcha et al. 2021). Exploring the different organs of *Zizyphus lotus* has shown its phytochemical richness in bioactive compounds (Berkani et al. 2022), and its biological activities (Hammi et al. 2022; Ait-Abderrahim et al. 2019). Environmentally, *Ziziphus Lotus* was tested according to what several studies bring for its capacity to eliminate cationic dyes (Boudechiche et al. 2019), to eliminate anionic dyes (El Messaoudi et al. 2022), cadmium ions (El Yakoubi et al. 2023a), lead ions (El Yakoubi et al. 2023b) consecutively. The best metal adsorption rate is obtained with a temperature ranging from 25°C to 30°C, a contact time of 90 min, an initial ionic concentration of 100 mg/L, and a biosorbent dosage ranging from 3.5 to 5 g/L. The experimental kinetic data of the biosorption process for both heavy metal ions were fitted by the pseudo-second-order model. The equilibrium data fitted very well to the Langmuir model and Temkin model. The maximum monolayer biosorption capacities were 70.78 and 80.75 mg/g for Cd(II, and to show an anticorrosive potential (Oukhrib et al. 2017).

Our present work aimed to evaluate the process of depolluting an aqueous solution containing Cr(VI) by *Zizphus lotus* fruit powder (ZLFP), while examining the effect of several parameters related to the reaction bath, the biosorbent particles, and the adsorbent Cr(VI). Pseudo-first order, pseudo-second order and Elovich models,

were used to study the kinetics of pollutant biosorption. Equilibrium data were examined using the Langmuir (L), Freundlich (F) and Temkin (T) isotherms. Additionally, biosorption was studied thermodynamically.

MATERIALS AND METHODS

Harvesting and preparing fruit

In September 2021, the *Ziziphus lotus* fruits were harvested from some shrubs, located east of Targuist in Morocco. With distilled water, the collected samples underwent several washes to remove debris. Subsequently, they were sun-dried and further dried in an electric oven at 60°C for 24 hours. An electric mixer was utilized to grind the samples into a fine powder. The resulting ZLFP was then directly poured into a glass beaker without any additional preparation steps.

Preparation of Cr(VI) solutions

By dissolving a mass of 2.828 g of $K_2Cr_2O_7$ in deionized water, a Cr (VI) stock solution was obtained. Consequently, a range of concentrations was achieved by performing sequential dilutions of the ionic stock solution.

Batch experiment of Cr(VI) biosorption

Biosorption experiments of Cr(VI) on the ZLFP sample were conducted in a batch system. The biosorption process was investigated with respect to various parameters, including pH, dosage of ZLFP, temperature, initial ions concentration, time of contact, and ZLFP particle size. The experiments were carried out in 500-ml Erlenmeyer flasks equipped with continuous agitation. Using a HANNA pH meter and either a 100 mmol/L HCl solution or a 100 mmol/L NaOH solution, the pH values were brought to the appropriate levels. Freshly prepared and diluted solutions were utilized for each experiment. All chemicals employed in the study were of the highest quality. Optimal parameters for better biosorption efficiency have been deduced by experimenting in ranges of pH (2-10), Temperature (15-50°C), ZLFP dosage (1-5 g/L), initial concentration (50-500 mg/g), particle size (Ø <100µm - Ø > 500 µm), and FP-Cr(VI) interaction time.

Analysis and characterization of samples

Assessment of elimination potential was based on the measurement of the Cr(VI) concentration before sorption process and after sorption process using a GBC 932 plus as an atomic absorption spectrophotometry. Equations (1) and (2) were used to estimate the adsorption capacity q_e (mg/g) and removal percentages (%R), consecutively, of Cr(VI) ions from aqueous solutions by the ZLFP.

$$q_e = \frac{C_i - C_e}{m} \quad (1)$$

$$(\%R) = \frac{C_i - C_e}{C_i} * 100 \quad (2)$$

where: C_i (mg/L) – initial Cr(VI) ions concentration, C_e (mg/L) – equilibrium Cr(VI) ions concentration, m (g/L) – concentration of *Zizphus lotus* fruit powder.

To explore the correlation between ZLFP particle size (PS) variable and specific surface area (SSA) variable in the powders, measurements of SSA were performed for various size ranges. The SSA of FP was determined using the Brunauer-Emmett-Teller (BET) method by the adsorption isotherms of N_2 at -196 °C (77 K) on an ASAP 2020, Micromeritics, USA. Prior to each test, the samples of FP underwent degassing at 433 K for 12 hours. FTIR spectroscopy was deployed using a Bruker Alpha equipment To determine different kinds of chemical functions present in each sample of ZLF. Thus, multiple discs of potassium bromide (KBr) were established, with each disc containing 1 mg of the ZLFP sample and 100 mg of KBr. FTIR spectra were obtained in the range of 400 to 4000 cm^{-1} with a detector resolution of 2 cm^{-1}.

By fixing the other parameters to their optimal values (particles size <100 µm, pH = 2, C_i = 100 mg/L, T (°C)= 30 °C, m = 5 g/L, and contact time = 600 min), the effect of each parameter is assessed.

RESULTS AND DISCUSSION

pH effect

The pH of the solution may have an impact on an adsorbent's characteristic adsorption sites, which would consequently affect the efficiency of adsorption in the process of removing pollutants contaminating wastewater. It has been shown

from several previous studies that the efficiency of Cr (VI) removal is strongly controlled by the pH of the ionic solution. The values of %R and q_e were estimated over a pH range (2–10) as shown in Figure 1. Thus, both the percentage removal (R) and the biosorption capacity (qe) are high in a remarkably acidic medium, and gradually decrease with increasing solution pH. The removal percentage and the biosorption capacity decrease from 94.30% to 24.9% and from 18.86 to 4.98 mg/g, when the pH of the solution increases from 2 to 10, respectively. Depending on the medium's pH and chromate content, Cr (VI) can exist as a variety of ionic species. Thus, in the pH range extending from 2 to 6, it is mainly the $Cr_2O_7^{2-}$ and $HCrO_4^-$ species that are found in solution, while for higher pH values the CrO_4^{2-} anions dominate (Rai 2023). A low pH of the ionic solution reflects a high concentration of H^+ ions, making the surface of the biosorbent positively charged, which allows attraction of the negatively charged chromium anions, and which could explain the greater percentage of elimination as well as the greater capacity of biosorption in an acid medium. With increasing pH, the medium becomes increasingly rich in OH^- ions, which compete with Cr (VI) anions, disfavoring biosorption, and which could therefore explain the low values of both elimination percentage and biosorption capacity at high pH values.

Biosorbent dosage effect

As a function of the ZLFP dose, the percentage of removal as well as the biosorption capacity of Cr(VI) were assessed. The obtained data are illustrated in Figure 2. When the dosage of the biosorbent increases from 1 to 5 g/L, the percentage of elimination of Cr(VI) increases from 40.36% to 94.30%, while the biosorption capacity drops from 40.36 to 18.86 mg/g, respectively. As the ZLFP dosage increases in solution, the number

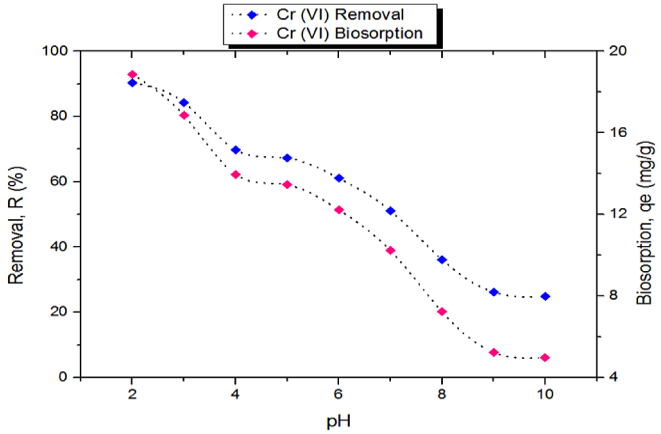

Figure 1. Evolution of the elimination percentage and biosorption capacity on *Zizphus lotus* fruit powder as a function of pH

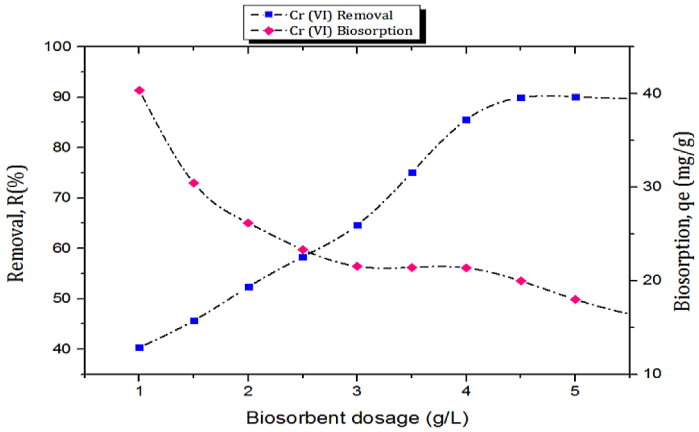

Figure 2. Biosorbent dosage effect on removal percentage and biosorption capacity onto *Zizphus lotus* fruit powder

of Cr(VI)-specific adsorption sites also increases, which could explain the intensification of the Cr(VI) removal process. Moreover, although the dosage of ZLFP has been gradually increased, the specific sites of adsorption of the anionic species of Cr(VI) are already saturated, which will only decrease the ratio described in equation (1), and which could hence explain the decrease in biosorption capacity (qe) with increasing amount of ZLFP.

Table 1. The particle size classe and specific surface area of *Zizphus lotus* fruit powder

Particle size classe (µm)	Specific surface area (m^2/g)
<100	2.022
100–300	1.657
300–500	1.325
>500	0.953

Effect of ZLFP particle size/time of contact

The biosorption of Cr(VI) were investigated for samples particles of various sizes, ranging from less than 100 µm to more than 500 µm, in relation to the time of interaction, as indicated in Figure 3. The data collected suggests that the biosorption kinetics of Cr(VI) is influenced by both the time of contact and size of ZLFP particles. The ZLFP sample whose size is less than 100 µm expresses a considerable equilibrium removal rate, increasing from 50.1% to 94.3% when the contact time increases from 60 min to 600 min. Clearly, it was the small ZLFP particles (Ø <100µm) that were able to offer the highest removal rate, and the percentage of chromium ion elimination increases with increasing ZLFP-Cr(VI) contact time. The results demonstrate that the removal efficiency of Cr(VI) increases as the size of the biosorbent particles decreases. The greater SSA that smaller biosorbent particles display helps to explain this observation, as shown in Table 1.

Because they are the most effective at eliminating Cr(VI) ions, particles smaller than 100 µm were used to study the effects of different parameters on the removal percentage and biosorption capacity.

Cr(VI) initial concentration effect

The impact of this parameter was evaluated in a range from 50 to 500 mg/L, as shown in Figure 4. The best chromium removal efficiency (from 94.30% to 92.89%) was obtained by using low initial ionic concentrations (from 50 to 200 mg/L, respectively). Thus, when the initial concentration increases from 50 to 500 mg/L, the elimination percentage regresses from 94.30% to 56.25%, while the biosorption capacity increases from 9.43 to 56.25 mg/g. When the concentration of Cr(VI) exceeds 150 mg/L, the active sites of adsorption on the surface of ZLFP would become saturated by the ionic species of Cr(VI), which become encumbered, and enter into repulsive molecular agitations destabilizing their sequestration by the surface of ZLFP, which could explain the fall in the percentage of elimination beyond 200 mg/L of the adsorbate. On the other hand, the saturation of the adsorption sites over low ranges of initial concentrations, and the variation of the

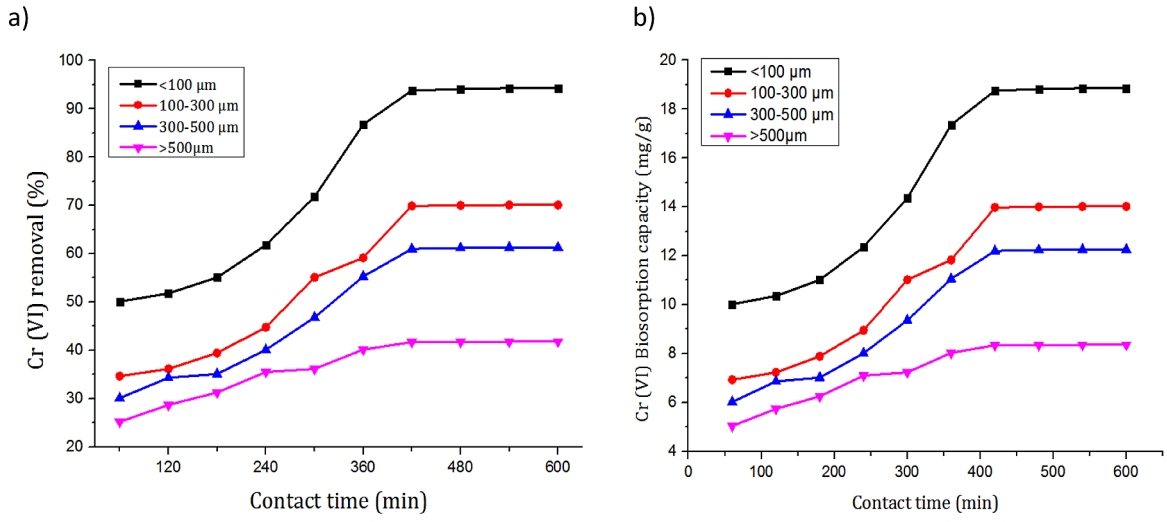

Figure 3. Effect of particle size/contact time, on removal percentage (a) and biosorption capacity (b) onto *Zizphus lotus* fruit powder

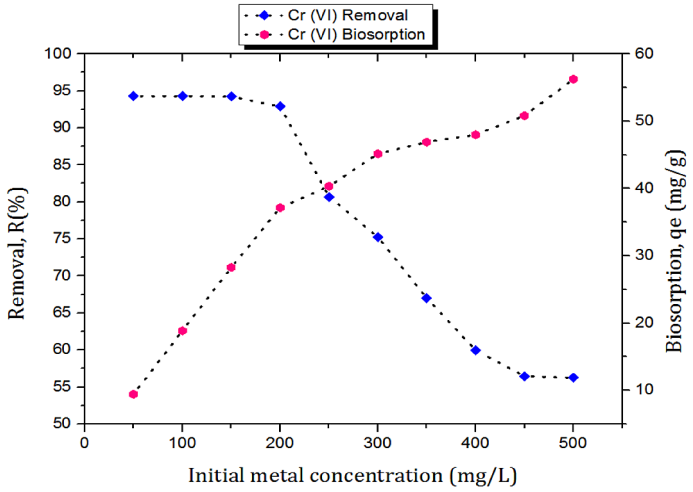

Figure 4. Effect of initial concentration on removal percentage and biosorption capacity onto *Zizphus lotus* fruit powder

biosorption capacity proportionally to the initial ionic concentration, as described in equation (1), could explain the gradual increase in adsorption capacity when the initial ionic concentration increases from 50 to 500 mg/L.

FTIR spectra analysis and characterization of ZLFP samples

To identify the most significant biological groups present in the biosorbent and their contribution during the Cr(VI) trapping process, FTIR spectra are employed as a qualitative study technique. This allowed to deduce the nature of the biochemical groups at the origin of the interaction coreing the Cr (VI) – ZLFP adsorption phenomenon.

The FTIR spectra (400 to 4000 cm^{-1}) for the unloaded sample and the Cr (VI) loaded sample are shown in Figure 5. The composition and molecular structure of the biomass employed have a major effect on the FTIR spectrum's shape (Alouache et al. 2022). The involvement of O-H groups (carboxylic acids, alcohols, and phenols), which are typical of pectins, lignin, and cellulose, is indicated by the broad high peak at 3432 cm^{-1} for ZLFP. The seen peaks at 2924 cm^{-1} would have been attributed to aliphatic acids' C-H stretching vibrations.

The peak noted at 1732 cm^{-1} in the FTIR spectra of the ZLFP sample would possibly be due to the stretching vibration of the C=O bond. This indicates the presence of carboxylic and esters groups in the ZLFP. The peak observed at 1160

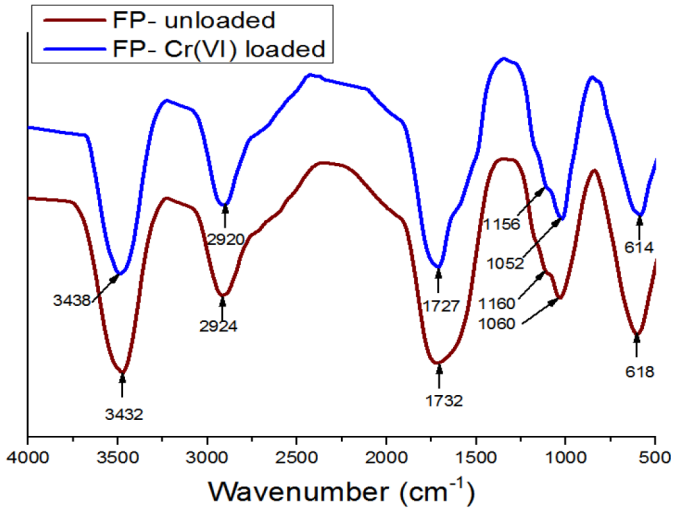

Figure 5. FTIR analysis of unloaded sample and the Cr(VI) loaded sample

cm^{-1} in the FTIR spectrum of the ZLFP biosorbent is likely attributed to the stretching of the C-O antisymmetric bridge in the cellulosic components of the biomass. The presence of lignin can be recognized by an absorption band at about 1060 cm^{-1} generated by the -O-CH_3 group in the Biosorbent sample. The bending modes of the aromatic compounds would produce a strong band at 618 cm^{-1}. The figure shows also that following the process of Cr(VI) biosorption, there is a significantly decrease in the intensities of the peaks, particularly those associated with hydroxyl and carboxyl radicals. Furthermore, slight shifts in the positions of these peaks are also noted. The abundantly available hydroxyl and carboxyl groups in sample biomass (ZLFP) have been demonstrated, in the FTIR spectra, to considerably contribute to the biosorption of Cr (VI) by electrostatic forces.

Biosorption kinetics

In order to understand the mechanism that governs the adsorption process, the experimental results were interpreted using the pseudo first order kinetic model (PFOK), the pseudo second order kinetic model (PSOK), and Elovich model. The kinetic data were exploited based on the regression coefficient (r^2) and the amount of Cr(VI) adsorbed per unit weight of ZLFP. The following equations (3), (4), and (5) give the expressions relating to PFOK, PSOK, and the Elovich model respectively:

$$q_t = q_e(1 - e^{-K_1 * t}) \tag{3}$$

$$\frac{t}{q_t} = \frac{1}{K_2 q_e^2} + \frac{t}{q_e} \tag{4}$$

$$q_t = \frac{1}{\beta} \operatorname{Ln}(1 + \alpha\beta t) \tag{5}$$

where: q_e – amount of Cr(VI) ions trapped at equilibrium (mg/g), q_t – amount of Cr(VI) ions trapped at any time *t*, (mg/g), K_1 – rate constant for the PFOK model, K_2 – rate constant for the PSOK model, α – initial adsorption rate (mg/g min), β – constant of desorption (g/mg).

Table 2 shows the kinetic data, as well as the correlation coefficients (r^2) relating to each of the models implemented. According to the kinetic parameters of Cr(VI) biosorption onto ZLFP provided by the three models, the correlation coefficients (r^2) for the PSOK and Elovich models are closer to 1 than the correlation coefficients provided by the PFOK model. Moreover, the experimental value of the biosorption capacity is closer to the value theoretically obtained by PSOK. It is evident that Cr(VI) biosorption kinetics onto ZLFP follows PSOK behavior, thus suggesting the predominant involvement of the chemisorption process, which is corroborated by the data from the Elovich model. Similar results were reported on Cr(VI) biosorption by *Phanera vahlii* (Ajmani et al. 2019), and *Ziziphus spinach-risti* (Mahmoud et al. 2021).

Biosorption isotherm

These are the Langmuir (L), Freundlich (F) and Temkin (T) models which were recruited to analyze the experimental data relating to Cr(VI) – ZLFP biosorption. Thus, The adsorbent-adsorbate contact surface is assumed to be homogeneous in the Langmuir model, with an identical adsorption sites, and the adsorption occurs in a monolayer fashion, where adsorbate molecules occupy the accessible surface adsorption sites. The model is described mathematically by equation (6):

$$q_e = q_m \frac{1 + K_L C_e}{K_L C_e} \tag{6}$$

where: q_e (mg/g), q_m (mg/g), K_L (L/mg), C_e (mg/L) – represent biosorbed quantity at equilibrium state, maximum adsorption capacity, Langmuir equilibrium constant, and equilibrium concentration of Cr(VI), respectively.

Table 2. Kinetic variables of Cr(VI) to *Zizphus lotus* fruit powder adsorption

Kinetic parameters		
Model	$q_{e,\,exp}$	18.86
PFOK	$q_{e,\,cal}$ (mg/g)	16.850
	K_1 (min^{-1})	0.010
	r^2	**0.986**
PSOK	$q_{e,\,cal}$ (mg/g)	20.307
	K_2 (g/mg·min)	5.42 E^{-4}
	r^2	**0.996**
Elovich	α (mg/g·min)	0.306
	β (g/mg)	0.195
	r^2	**0.992**

The multilayer arrangement of the adsorbate on a heterogeneous surface of the adsorbent is described by the Freundlich isotherm according to formula (7) presented below:

$$q_e = K_F C_e^{1/n} \quad (7)$$

where: K_F – Freundlich constant ($mg^{1-1/n}\, g^{-1}\, L^{1/n}$), n – a heterogeneity factor, $1/n$ – relating to the biosorption intensity.

The model which best corresponds to the experimental data recorded is the one having offered the value of the correlation coefficient (r^2) closest to 1. By studying Cr(VI) – ZLFP interactions, the Temkin model suggests that due to repulsive molecular interactions, the molecular adsorption heat of the layer decreases linearly with coverage, as expressed mathematically by equation (8):

$$q_e = \frac{RT}{B} \text{ Ln } (A\, C_e) \quad (8)$$

As illustrated in Figures 6–7, the biosorption capacities of ZLFP for Cr(VI) were studied for various initial metal concentrations. The experimental results show that the biosorption capacity increases as the Cr(VI) concentration in the reaction media increases.

The trend of an increase in biorption capacity with an increase in Cr(VI) concentration could be explained by strong driving forces for mass movement (Khalil et al. 2020). The probability of a dissolved species binding to an adsorbent rises with the concentration increase of that species in the aqueous solution. Consequently, the biosorption capacity is determined by the initial metal concentration (Bayuo et al. 2019). The isotherms express an L-type shape characteristic of the Giles classification (Prabhakaran et al. 2019). Such an isotherm suggests that the competition between water molecules and Cr(VI) ions would be minimal in current conditions (Ugraskan et al. 2022). The adsorption isotherm models (L), (F), and (T) have been compared to the experimental isotherms. Table 3 shows the adsorption parameters and correlation coefficients associated with each isotherm model. Through comparison, it is possible to assess how well each model corresponds to the actual data and understand more about the system behavior and biosorption mechanism. Referring to the r^2 values, it turns out that the model (L) provided the most accurate fit to the experimental data, suggesting that Cr(VI) ions are uniformly adsorbed on a ZLFP monolayer surface, with a maximum capacity of biosorption of 36.11 ± 1.52 mg/g.

A comparison was made between the ZLFP's biosorption capacity and results of earlier research on the sequestration of Cr (VI) by plant biomass. As seen in Table 4, the biosorbent potential of ZLFP has been demonstrated by this research to be significantly higher than that of a number of biosorbents mentioned in the literature. The significant biosorption potential of ZLFP makes this biomass an efficient and cost-effective tool that can be applied to wastewater to remove Cr (VI).

Elution and regeneration

Elution and regeneration are important steps in the biosorption process. Understanding the phenomenon is crucial on the one hand for the

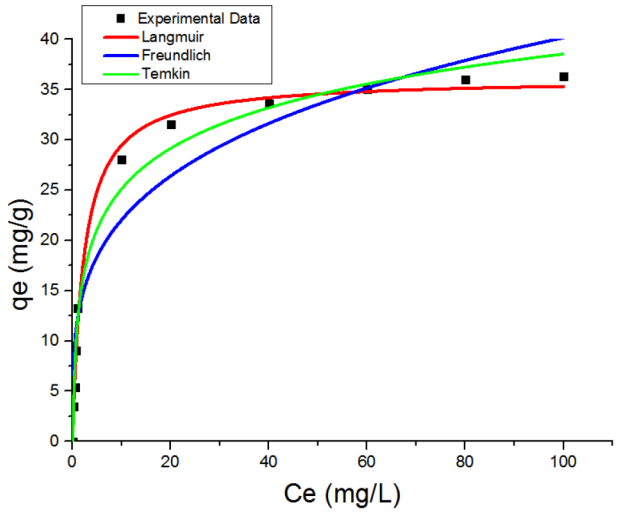

Figure 6. Langmuir (L), Freundlich (F) and Temkin (T) isotherms of Cr(VI) biosorption onto ZLFP

Table 3. Constants of isotherms: Langmuir (L), Freundlich (F) and Temkin (T), that characterize the adsorption of Cr(VI) onto ZLFP

Isotherms constants		
Langmuir (L)	q_m (mg/g)	36.11 ± 1.52
	K_L (L/mg)	0.443 ± 0.023
	r^2	**0.994**
Freundlich (F)	K_F ($mg^{1-1/n} g^{-1} L^{1/n}$)	12.099 ± 1.098
	n	0.260 ± 0.019
	r^2	0.908
Temkin (T)	A (L/g)	7.415 ± 0.555
	B	5.830 ± 1.012
	r^2	**0.984**

Table 4. Maximum biosorption capacity of ZLFP for Cr(VI) compared to other environmentally friendly biosorbents

Biosorbents	q_m (mg/g) Cr(VI)	References
Date palm fruit	70.49	[47]
Bael fruit	17.27	[48]
Magnolia leaf	12.3	[49]
Mangrove leaf powder	54.34	[50]
Aspergillus fumigatus	45.5	[51]
Oak wood char	3.03	[52]
Rhizopus. sp	9.95	[53]
Gliricidia sepium leaf powder	33.57	[54]
Ziziphus lotus (fruits)	36.11	Present study

recovery of adsorbed substances, and on the other hand, for the regeneration of the biosorbent, its preparation for subsequent use, and the extension of its lifespan. Using HCl (0.20 M), as eluent for Cr(VI), and in four consecutive cycles, ZLFP was regenerated, still retaining eliminatory power against hexavalent chromium. According to this result, the use of ZLFP as an efficient and economically affordable biosorbent is recommended.

Temperature effect and thermodynamic study

The influence of temperature on the biosorption of Cr(VI) onto ZLFP was studied in the temperature range of 15–50°C as shown in Figure 7. The biosorption potentiel increases with the increase in the temperature of the medium. Thus, from 30°C the quantity of Cr(VI) adsorbed increases slightly. The increase in the biosorption rate is explained by the fact that as the medium's temperature rises, molecular agitation also rises.

To comprehend the thermodynamic traits of the biosorption Cr(VI) to *Zizphus lotus* fruit powder, the following equations were utilized to compute several parameters, including ΔG°, ΔH°, and ΔS°:

$$K_d = \frac{q_e}{C_e} \tag{9}$$

$$\Delta G = \Delta H - T\Delta S \tag{10}$$

$$Ln\, K_d = \frac{\Delta S}{R} - \frac{\Delta H}{RT} \tag{11}$$

where: K_d – distribution coefficient (mL/g), ΔH – enthalpy change (kJ/mol), ΔG – Gibbs free energy change (kJ/mol), ΔS – entropy change (J/mol·K), R – universal gas constant (8.314 J/ mol·K), T – temperature (K).

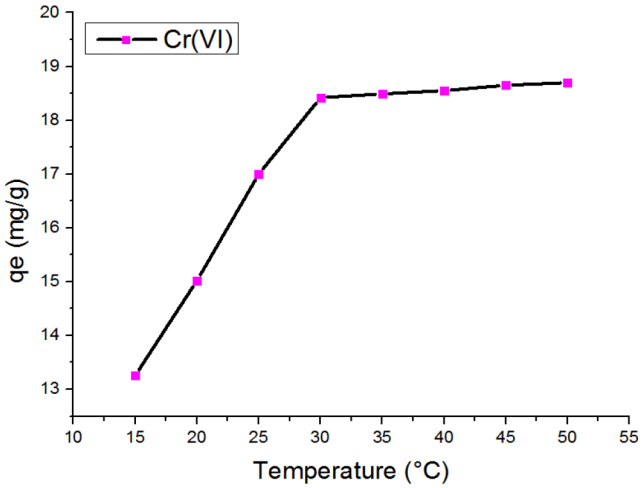

Figure 7. Temperature effect on Cr(VI) elimination by ZLFP

Table 5. Thermodynamic parameters estimated for the biosorption of Cr(VI) by *Zizphus lotus* fruit powder

Heavy metal	T (K)	K_d	ΔG^0(KJ/mol)	ΔH°(kJ/mol)	ΔS°(J/K mol)
Cr(VI)	293	17.67	- 20.39	- 6.69	46.76
	303	22.58	- 20.86		
	313	22.77	- 21.32		
	323	23	- 21.79		

Using the slopes and intercepts of the linear regression of Ln $K_d = f(1/T)$, the thermodynamic variables were estimated and indicated in Table 5.

The negative values of ΔH° (ΔH° = - 6,69 kJ/mol) suggest that the chemical process is exothermic and the positive values of entropy ΔS° (ΔS° = 46,76 J/K mol) suggest a considerable Cr(VI) affinity for ZLFP. Moreover, the Gibbs free energy (ΔG°) is negative, and it decreases when the temperature increases from 293 to 323 K, which confirms the feasibility of the biosorption and the spontaneous nature of the process.

CONCLUSIONS

The main aim of the current work was to examine the use of *Ziziphus lotus* fruits as a biosorbent in the removal of Cr(VI) ions from an ionic solution. Conventional methods for eliminating Cr(VI) ions from wastewater are known to be costly, making the utilization of *ziziphus lotus* fruits an attractive alternative. The biosorption capacity was found to be strongly affected by factors such as ZLFP dosage, particle size, temperature, initial Cr(VI) concentration, pH, and contact time. The characterization of ZLFP material using the BET method revealed that particles smaller than 100 µm exhibited the highest specific surface area, indicating their suitability for enhanced metal ion adsorption. Kinetic and isothermal modeling of the data collected suggested that the Cr(VI) biosorption could be well described by the PSOK model and the Langmuir isotherm respectively. The maximum capacity of biosorption (q_m), calculated from the model of Langmuir, was found to be 36.11 mg/g.

The study of the Cr(VI) to *Zizphus lotus* fruit powder elution-regeneration process demonstrated the capacity of ZLFP to preserve the biosorbent character after 4 consecutive cycles. Although few studies reporting biosorption technology transfer from laboratory scale to large application scale, the successful application of the biosorption method using *ziziphus lotus* fruits suggests its potential use in different water treatment processes in terms of Cr(VI), offering an alternative to conventional methods.

REFERENCES

1. Abcha I., Ben-Haj Said L., Salmieri S., Criado P., Neffati M., Lacroix M. 2021. Optimization of extraction parameters, characterization and assessment of bioactive properties of *Ziziphus lotus* fruit pulp for nutraceutical potential. European Food Research and Technology, 247(9), 2193-2209.
2. Abdul M.K.N., Fitri A., Wan-Mohtar W.H.M., Wan-Mohd J.W.S., Zuhairi N.Z., Kamarudin M.K.A. 2021. A study of spatial and water quality index during dry and rainy seasons at Kelantan River Basin, Peninsular Malaysia. Arab J Geosci, 14 (2), 852021.
3. Ait-Abderrahim L., Taïbi K., Ait-Abderrahim C. 2019. Assessment of the Antimicrobial and Antioxidant Activities of *Ziziphus lotus* and *Peganum harmal*a. Iranian Journal of Science and Technology, Transactions A: Science, 43, 409-414.
4. Ajmani A., Shahnaz T., Subbiah S., Narayanasamy S. 2019. Hexavalent chromium adsorption on virgin, biochar, and chemically modified carbons prepared from *Phanera vahlii* fruit biomass: Equilibrium, kinetics, and thermodynamics approach. Environmental Science and Pollution Research, 26, 32137-32150.
5. Akpomie K.G., Conradie J. 2020. Banana peel as a biosorbent for the decontamination of water pollutants. Environ Chem Lett, 8(4), 1085–1112.
6. Alouache A., Selatnia A., Sayah H.E., Khodja M., Moussous S., Daoud N. 2022. Biosorption of hexavalent chromium and Congo red dye onto Pleurotus mutilus biomass in aqueous solutions. International Journal of Environmental Science and Technology, 19(4), 2477-2492.
7. Anandkumar J., Mandal B. 2009. Removal of Cr(VI) from aqueous solution using Bael fruit (*Aegle marmelos correa*) shell as an adsorbent. Journal of Hazardous Materials, 168(2), 633–640.
8. Arola K., Van-der-Bruggen B., Mänttäri M., Kallioinen M. 2019. Treatment options for nanofiltration and reverse osmosis concentrates from municipal

wastewater treatment: A review. Critical Reviews in Environmental Science and Technology, 49(22), 2049–2116.

9. Ayele A., Godeto Y.G. 2021. Bioremediation of chromium by microorganisms and its mechanisms related to functional groups. Journal of Chemistry, 1–21.
10. Bayuo J., Pelig-Ba K.B., Abukari M.A. 2019. Adsorptive removal of chromium (VI) from aqueous solution unto groundnut shell. Applied Water Science, 9(4), 107.
11. Berkani F., Dahmoune F., Kadri N., Serralheiro M.L., Ressaissi A., Abbou., et al. 2022. LC–ESI–MS/MS analysis, biological effects of phenolic compounds extracted by microwave method from Algerian *Zizyphus lotus* fruits. Food Measure, 16(5), 3354–3371.
12. Boloy R.A.M., Da-Cunha R.A., Rios E.M., De-Araújo S.M.J., Soares L.O., Machado V. A., et al. 2021. Waste-to-energy technologies towards circular economy: A systematic literature review and bibliometric analysis. Water Air Soil Pollut, (7) 306.
13. Boudechiche N., Fares M., Ouyahia S., Yazid H., Trari M., Sadaoui Z. 2019. Comparative study on removal of two basic dyes in aqueous medium by adsorption using activated carbon from *Ziziphus lotus* stones. Microchemical Journal, 146, 1010–1018.
14. Butnariu M. 2022. Heavy metals as pollutants in the aquatic Black Sea ecosystem. Bacterial Fish Diseases, Academic Press, 31–57.
15. Chai W.S, Cheun J.Y, Kumar P.S, Mubashir M., Majeed Z., Banat F. et al. 2021. A review on conventional and novel materials towards heavy metal adsorption in wastewater treatment application. Journal of Cleaner Production, 296: 126589.
16. Coetzee J. J., Bansal N., and Chirwa E.M.N. 2020. Chromium in environment, its toxic effect from chromite-mining and ferrochrome industries, and its possible bioremediation. Exposure and Health, 12, 51-62.
17. Dhal B, Pandey, Abhilash B.D. 2018. Mechanism elucidation and adsorbent characterization for removal of Cr(VI) by native fungal adsorbent, Sustainable Environment Research, 28(6), 289–297.
18. El Maaiden E., El Kharrassi Y., Moustaid K., Essamadi A.K., Nasser B. 2019. Comparative study of phytochemical profile between *Ziziphus spina-christi* and *Ziziphus lotus* from Morocco. Food Measure, 13(1), 21–130.
19. El Messaoudi N., El Khomri M., Chegini Z.G., Bouich A., Dbik A., Bentahar S., et al. 2022. Dye removal from aqueous solution using nanocomposite synthesized from oxalic acid-modified agricultural solid waste and $ZnFe_2O_4$ nanoparticles. Nanotechnol. Environ. Eng., 7(3), 797–811.
20. El Yakoubi N., Ennami M., El Ansari Z. N., Ait-Lhaj F., Bounab L., El Kbiach M., et al. 2023a. Utilization of *Ziziphus lotus* fruit as a potential biosorbent for lead (II) and cadmium (II) ion removal from aqueous solution. Ecological Engineering & Environmental Technology, 24(3), 135–146.
21. El Yakoubi N., Ennami M., El Ansari Z.N., Ait-Lhaj F., Bounab L., El Kbiach M., et al. 2023b. Removal of Cd(II) and Pb(II) from aqueous solution using Ziziphus lotus leaves as a potential biosorbent, Desalination and Water Treatment. (300), 65–74.
22. Elahi A., Arooj I., Bukhari D.A., Rehman A. 2020. Successive use of microorganisms to remove chromium from wastewater. Appl Microbiol Biotechnol, 104(9), 3729–3743.
23. Elgarahy A.M., Elwakeel K.Z., Mohammad S.H., Elshoubaky G.A. 2021. A critical review of biosorption of dyes, heavy metals and metalloids from wastewater as an efficient and green process. Cleaner Engineering and Technology, 100209.
24. Espinoza-Sánchez M.A., Arévalo-Niño K., Quintero-Zapata I., Castro-González I., Almaguer-Cantú V. 2019. Cr(VI) adsorption from aqueous solution by fungal bioremediation based using *Rhizopus* sp. Journal of Environmental Management, 251, 109-595.
25. Hammi K. M., Essid R., Khadraoui N., Ksouri R., Majdoub H., Tabbene O. 2022. Antimicrobial, antioxidant and antileishmanial activities of Ziziphus lotus leaves. Archives of Microbiology, 204(1), 119.
26. Hube S., Eskafi M., Hrafnkelsdóttir K. F., Bjarnadóttir B., Bjarnadóttir M.Á., Axelsdóttir S., et al. 2020. Direct membrane filtration for wastewater treatment and resource recovery: A review. Science of The Total Environment, 710, 136375.
27. Jayakumar V., Govindaradjane S., Rajamohan N., Rajasimman M. 2021. Biosorption potential of brown algae, Sargassum polycystum, for the removal of toxic metals, cadmium and zinc. Environ Sci Pollut Res, 29(28), 41909–41922.
28. Jorge N., Santos C., Teixeira A.R., Marchão L., Tavares P.B., Lucas M.S., et al. 2022. Treatment of agro-industrial wastewaters by coagulation-flocculation-decantation and advanced oxidation processes – A literature review. Engineering Proceedings, 19(1), 33.
29. Khalil U., Shakoor B.M., Ali S., Rizwan M., Nasser A.M., Wijaya L. 2020. Adsorption-reduction performance of tea waste and rice husk biochars for Cr(VI) elimination from wastewater. Journal of Saudi Chemical Society, 24(11), 799–810.
30. Liu X., Tian R., Ding W., He Y., Li H. 2019. Adsorption selectivity of heavy metals by Na-clinoptilolite in aqueous solutions. Adsorption, 25(4) ,747–755.
31. Mahmoud A.E.D., Fawzy M., Hosny G., Obaid A. 2021. Equilibrium, kinetic, and diffusion models of chromium(VI) removal using Phragmites australis and *Ziziphus spina-christi* biomass. International

Journal of Environmental Science and Technology, 18, 2125-2136.

32. Mishra S., Bharagava R.N., More N., Yadav A., Zainith S., Mani S., et al. 2019. Heavy metal contamination: An alarming threat to environment and human health. Environmental Biotechnology: For Sustainable Future, 103–125.
33. Mohan D., Rajput S., Singh V.K., Steele P.H., Pittman C.U. 2011. Modeling and evaluation of chromium remediation from water using low cost bio-char, a green adsorbent. Journal of Hazardous Materials, 188: 319–333.
34. Mondal N.K., Samanta A., Roy P., Das B. 2019. Optimization study of adsorption parameters for removal of Cr(VI) using Magnolia leaf biomass by response surface methodology. Sustainable Water Resources Management, 5, 1627-1639.
35. Murtaza G., Shehzad M., Kanwal T., Farooqi U.R., Owens G. 2022. Biomagnification of potentially toxic elements in animals consuming fodder irrigated with sewage water. Environ Geochem Health, 44(12), 4523–4538.
36. Mushtaq Z., Liaquat M., Anum N., Liaquat R., Hira I., Waheed A., et al. 2022. Potential of plant growth promoting rhizobacteria to mitigate chromium contamination. Environmental Technology & Innovation, 28, 102826.
37. Oukhrib R., Issami E., Ibrahimi B., Mouaden K., Bazzi L. 2017. *Ziziphus lotus* as green inhibitor of copper corrosion in natural sea water. Portugaliae Electrochimica Acta, 35(4), 187–200.
38. Oyewole O.A., Zobeashia S.S.L.-T., Oladoja E.O., Raji R.O., Odiniya E.E., Musa A.M. 2019. Biosorption of heavy metal polluted soil using bacteria and fungi isolated from soil. SN Applied Sciences, 1, 1-8.
39. Parashar D., Gandhimathi R. 2022. Zinc Ions adsorption from aqueous solution using raw and acid-modified orange peels: Kinetics, Isotherm, Thermodynamics, and Adsorption mechanism. Water Air Soil Pollut, (233) ,10-400.
40. Prabhakaran D.C., Bolaños-Benitez V., Sivry Y., Gelabert A., Riotte J., Subramanian S. 2019. Mechanistic studies on the bioremediation of Cr(VI) using Sphingopyxis macrogoltabida SUK2c, a Cr(VI) tolerant bacterial isolate. Biochemical Engineering Journal, 107-292.
41. Rai R., Aryal R.L., Paudyal H., Gautam S. K., Ghimire K.N., Pokhrel M.R., et al. 2023. Acid-treated pomegranate peel; An efficient biosorbent for the excision of hexavalent chromium from wastewater. Heliyon, 9(5).
42. Rambabu K., Bharath G., Banat F., Show P.L. 2020. Biosorption performance of date palm empty fruit bunch wastes for toxic hexavalent chromium removal. Environmental Research, 109-694.
43. Rashid R., Shafiq I., Akhter P., Iqbal M.J., Hussain M., A state-of-the-art review on wastewater treatment techniques: the effectiveness of adsorption method. Environ Sci Pollut Res, 28(8), 9050–9066.
44. Rosinger A.Y., and Brewis A., 2019. Life and death: Toward a human biology of water. American Journal of Human Biology, 32(1).
45. Saatsaz M. 2020. A historical investigation on water resources management in Iran. Environment. Development and Sustainability, 22, 1749-1785.
46. Sadeghi H., Fazlzadeh M., Zarei A., Mahvi A.H., Nazmara S. 2022. Spatial distribution and contamination of heavy metals in surface water, groundwater and topsoil surrounding Moghan's tannery site in Ardabil, Iran. International Journal of Environmental Analytical Chemistry, 102(5), 1049-1059.
47. Sathish T., Vinithkumar N.V., Dharani G., Kirubagaran R. Efficacy of mangrove leaf powder for bioremediation of chromium (VI) from aqueous solutions: kinetic and thermodynamic evaluation. Applied Water Science, 5, 153-160.
48. Suganya E., Saranya N., Patra C., Varghese L. A., Selvaraju N. 2019. Biosorption potential of *Gliricidia sepium* leaf powder to sequester hexavalent chromium from synthetic aqueous solution. Journal of Environmental Chemical Engineering, 7(3), 103112.
49. Tariq M., Anayat A., Waseem M., Rasool M.H., Zahoor M.A., Ali S. et al. 2020. Physicochemical and bacteriological characterization of industrial wastewater being discharged to surface water bodies: Significant threat to environmental pollution and human health. Journal of Chemistry, 1–10.
50. Ugraskan V., Isik B., Yazici O., Cakar F. 2022. Removal of Safranine T by a highly efficient adsorbent (*Cotinus coggygria* leaves): Isotherms, kinetics, thermodynamics, and surface properties. Surfaces and Interfaces, 28, 101615.
51. Vu X.H., Nguyen L.H., Van H.T., Nguyen D.V., Nguyen T.H., Nguyen Q.T. et al. 2019. Adsorption of chromium (VI) onto freshwater snail shell-derived biosorbent from aqueous solutions: Equilibrium, kinetics, and thermodynamics. Journal of Chemistry, 1–11.
52. Wani A.A., Khan A.M., Manea Y.K., Salem M.A.S., Shahadat M. 2021. Selective adsorption and ultrafast fluorescent detection of Cr(VI) in wastewater using neodymium doped polyaniline supported layered double hydroxide nanocomposite. Journal of Hazardous Materials, 416, 125-754.
53. White L.M., Shibuya T., Vance SD., Christensen LE., Bhartia R., Kidd R., et al. 2020. Simulating serpentinization as it could apply to the emergence of life using the JPL hydrothermal reactor. Astrobiology, 20(3), 307–326.
54. Zhang Y., Duan X., 2020. Chemical precipitation of heavy metals from wastewater by using the synthetical magnesium hydroxy carbonate. Water Science and Technology, 81(6), 1130–1136.